Supporting Information

NaCl interphase enables stable $Na_{2.85}Sb_{0.95}W_{0.05}S_{3.9}Cl_{0.1}$-based all-solid-state sodium batteries

Zhanyou Feng[a,c], Liang Zhu[a], Enbo Qin[a], Ziman Weng[a], Jinghua Wu[a,b], Yong Li[a,b] and Xiayin Yao[a,b*]*

[a]Ningbo Institute of Materials Technology and Engineering, Chinese Academy of Sciences, Ningbo 315201, P. R. China

[b]Center of Materials Science and Optoelectronics Engineering, University of Chinese Academy of Sciences, Beijing, 100049 P. R. China

[c]Nano Science and Technology Institute, University of Science and Technology of China, Suzhou 215123, P. R. China

EXPERIMENTAL SECTION

1. Preparation of sodium solid electrolytes

Solid electrolytes of Na_3SbS_4, $Na_{3-x}Sb_{1-x}W_xS_4$ (x = 0, 0.025, 0.05, 0.075, and 0.1) and $Na_{2.95-x}Sb_{0.95}W_{0.05}S_{4-x}Cl_x$ (x = 0, 0.05, 0.1, 0.15, 0.2) were synthesized using a melt-quenching method followed by annealing process. The raw materials included Na_2S (95%, Aladdin Chemistry Co., Ltd.), Sb_2S_3 (99.9%, Aladdin Chemistry Co., Ltd.), S (99.95%, Aladdin Chemistry Co., Ltd.), WS_2 (99.9%, Aladdin Chemistry Co., Ltd.), and NaCl (99.9%, Aladdin Chemistry Co., Ltd.). According to the composition of different solid electrolytes, the corresponding raw materials were weighted mixed in an agate mortar for 20 minutes. To facilitate the oxidation of Sb^{3+} in Sb_2S_3, an additional 5 wt% of S was added. Subsequently, the mixture was heated in a sealed quartz tube at 600 ^oC for 2 hours and then rapidly quenched in iced water. The resulting precursor was pressed into pellets with a diameter of 10 mm and a thickness of approximately 1 mm under a pressure of 360 MPa, followed by annealing at 280 ^oC for 2 hours.

2. Characterizations

X-ray powder diffraction (XRD) was performed on a Bruker D8 Advance diffractometer with Cu K_α radiation (λ = 1.54178 Å) to identify the crystalline phases over a 2θ range of 10-80°. The XRD patterns were refined using the Rietveld method with the HighScore Plus (v4.8) software. The initial structural model based on Na_3SbS_4 (space group $P\bar{4}2_1c$) was adopted for the refinement. The background was fitted using a polynomial function, and the peak shape profile function was Pseudo-Voigt. The reliability criteria for refinement were assessed as follows: R_{wp}＜10%，R_p＜10%，the

Goodness of fit (χ^2)＜2.

Raman spectroscopy measurements were performed using Renishaw Via Reflex Raman spectrophotometer equipped with a 532 nm laser source. The surface chemical valence state of the solid electrolytes and the interfacial products between the solid electrolyte and sodium metal after symmetric cell cycling were analyzed using X-ray photoelectron spectroscopy (XPS, instrument model Axis UltraDLD, Kratos). The microstructure and elemental distribution of the samples were examined by scanning electron microscopy (SEM, Hitachi S-4800) coupled with energy-dispersive X-ray spectroscopy (EDS).

To evaluate the ionic conductivity, 200 mg of the electrolyte powder was cold-pressed into a pellet with a diameter of 10 mm and sandwiched between two carbon electrodes as an ionic blocking layer. Electrochemical impedance spectroscopy (EIS, Solartron 1470E) was conducted over a frequency range of 1 MHz to 10 Hz within a temperature range of -20 ^{o}C to 80 ^{o}C. Additionally, the electronic conductivity was determined by direct current polarization testing.

Density Functional Theory (DFT) calculations were performed using the CP2K packag[S1], employing the mixed Gaussian and plane-wave scheme[S2] and the Quickstep module[S3]. The Perdew-Burke-Ernzerhof (PBE) exchange correlation functional[S4], Goedecker-Teter-Hutter (GTH) pseudopotential[S5], DZVP-MOLOPT-SR-GTH / TZVP-MOLOPT-SR-GTH / TZVP-MOLOPT-GTH basis sets were used to describe the system[S2]. A plane-wave energy cut-off and relative cut-off of 400 Ry and 55 Ry were employed, respectively. The energy convergence criterion was set to 10^{-6} Hartree.

The DFT-D3(BJ) dispersion correction was applied to account for long-range van der Waals interactions[S6]. Structural optimization was carried out using the Limited Memory Broyden-Fletcher-Goldfarb-Shannon (LBFGS) optimizer, until the maximum force was below 0.00045 Ry/Bohr (0.011 eV/Å). 3 ×3×3 supercells were used to build the model cells and incorporate the W-Cl substitution. The cell was first relaxed, followed by ionic relaxation under the Nose-Hoover thermostat (NVT ensemble) to achieve energy optimization.

To evaluate the chemical stability of the solid electrolyte in humid air, 200 mg of the sample was placed in a sealed container with a volume of 2100 cm^3. The container was filled with air at a relative humidity of 45% and maintained at a constant temperature of 30°C. Real-time monitoring of gas release was conducted using an H_2S sensor, and the corresponding H_2S release profile was plotted.

3. Evaluation of all-solid-state sodium batteries

All-solid-state sodium batteries were assembled with metallic sodium as the anode and a composite electrode as the cathode. Commercial TiS_2 was subjected to high energy ball-milling to reduce its particle size to several hundred nanometers[S7]. The solid electrolyte layer was prepared by cold-pressing approximately 200 mg of solid electrolyte powder at 90 MPa. The electrode material of approximately 1.0 mg cm^{-2} was evenly spread on one side of the solid electrolyte layer and pressed at 180 MPa. Finally, a Na metal foil was attached to the opposite side of the solid electrolyte layer. The obtained all solid-state battery were secured with nuts and screws and tested over a voltage range of 1.0 to 2.5 V at 25 °C using a multi-channel testing system (LAND

CT-2001A, Wuhan Lambo Testing Equipment Co., Ltd.).

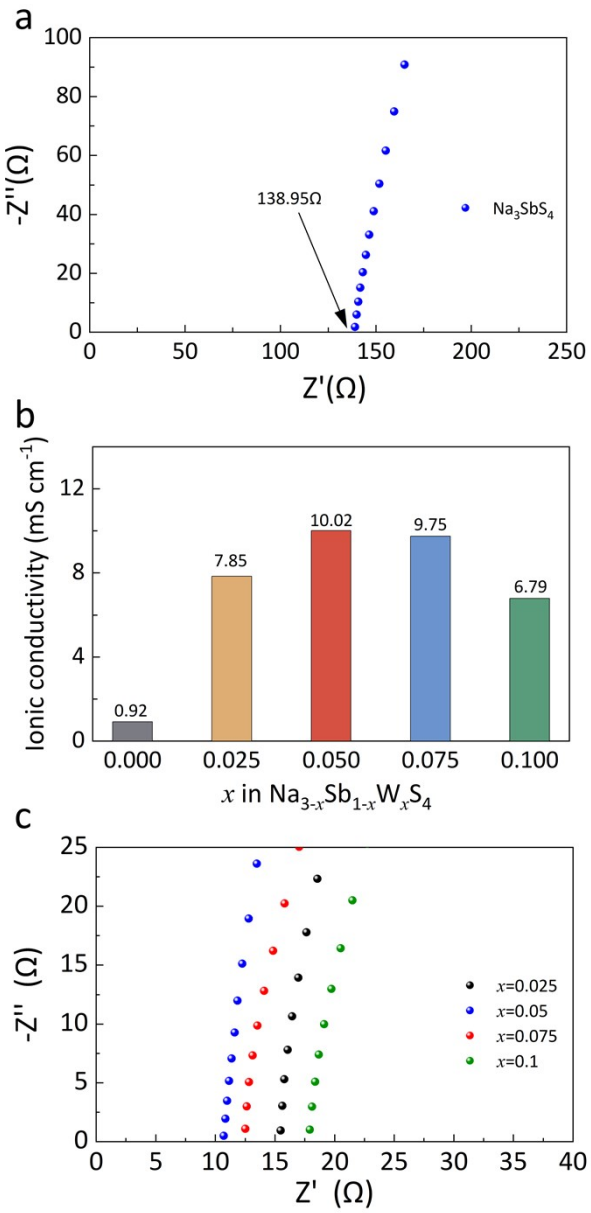

Figure S1. (a) Nyquist plots of Na_3SbS_4 solid electrolyte. (b) Ionic conductivities of the $Na_{3-x}Sb_{1-x}W_xS_4$ (x = 0, 0.025, 0.05, 0.075 and 0.1) solid electrolytes and (c) Nyquist plots of the $Na_{3-x}Sb_{1-x}W_xS_4$ (x = 0.025, 0.05, 0.075 and 0.1) solid electrolytes.

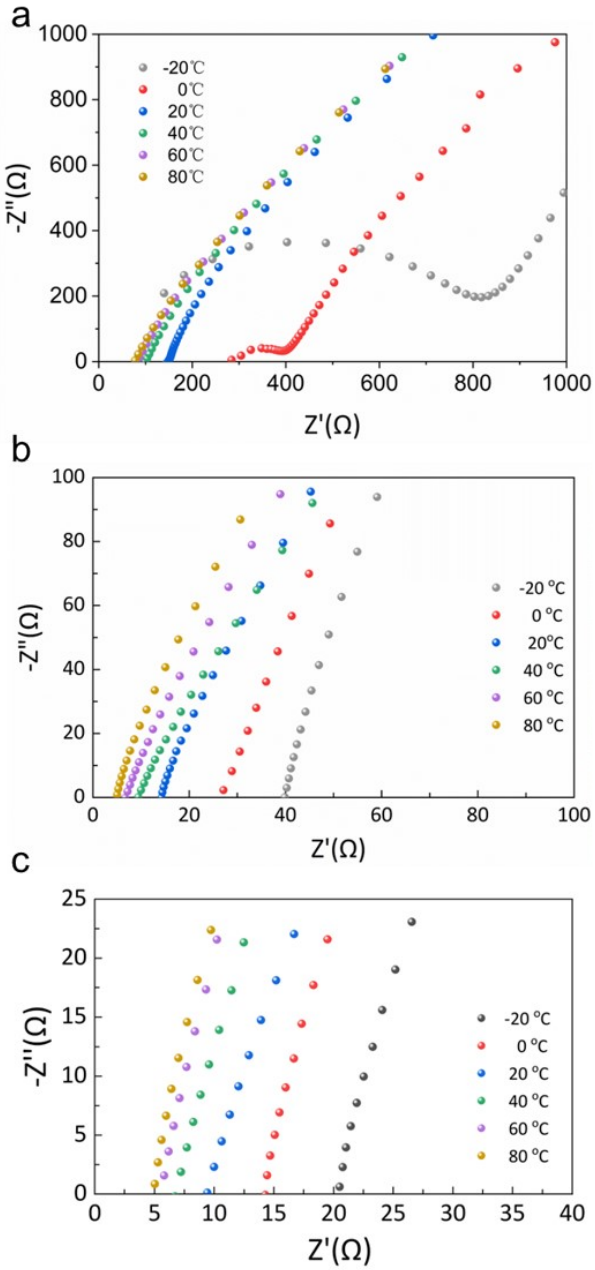

Figure S2. Nyquist plots of (a) Na_3SbS_4, (b) $Na_{2.95}Sb_{0.95}W_{0.05}S_4$ and (c) $Na_{2.85}Sb_{0.95}W_{0.05}S_{3.9}Cl_{0.1}$ under different temperatures.

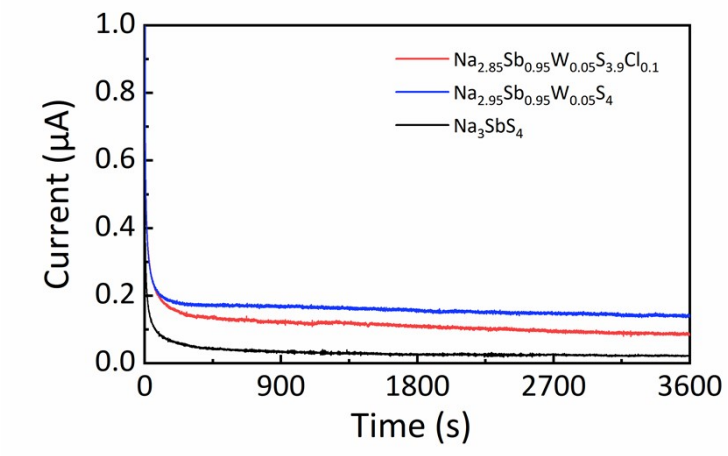

Figure S3. Current-time curves of the C/electrolytes/C cells with Na_3SbS_4, $Na_{2.95}Sb_{0.95}W_{0.05}S_4$ and $Na_{2.85}Sb_{0.95}W_{0.05}S_{3.9}Cl_{0.1}$ solid electrolytes.

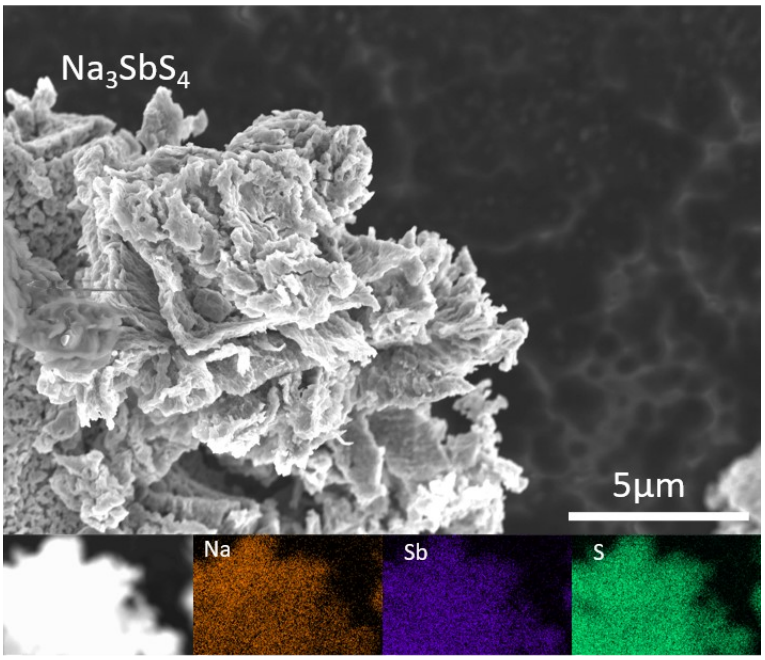

Figure S4. SEM image and corresponding elemental mapping images of the Na_3SbS_4 solid electrolyte.

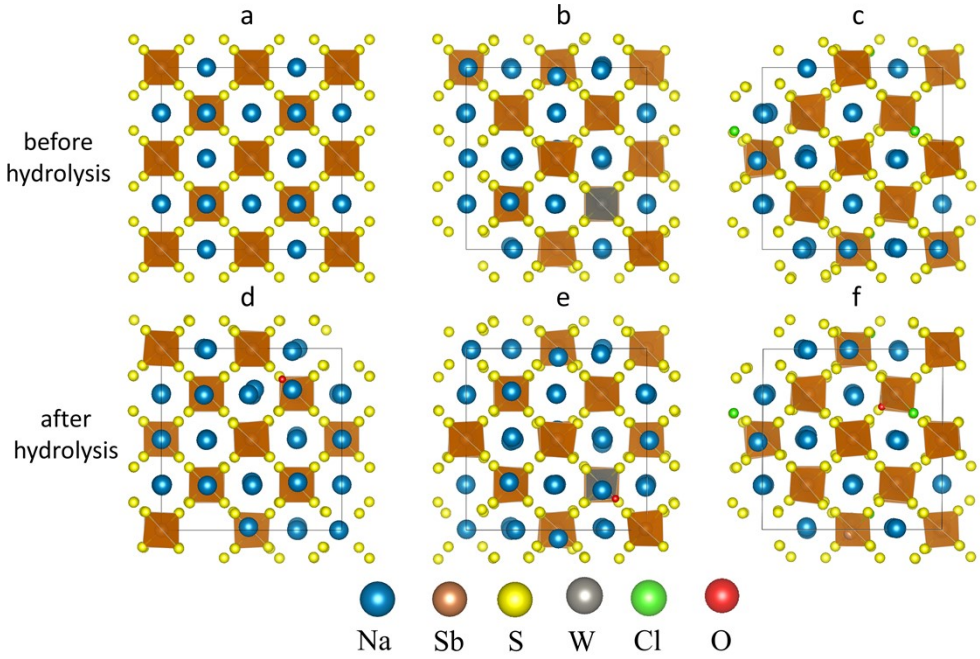

Figure S5. Optimized crystal structures before and after hydrolysis for (a, d) Na_3SbS_4, (b, e) $Na_{2.95}Sb_{0.95}W_{0.05}S_4$ and (c, f) $Na_{2.85}Sb_{0.95}W_{0.05}S_{3.9}Cl_{0.1}$, where partial sulfur atoms are replaced by oxygen.

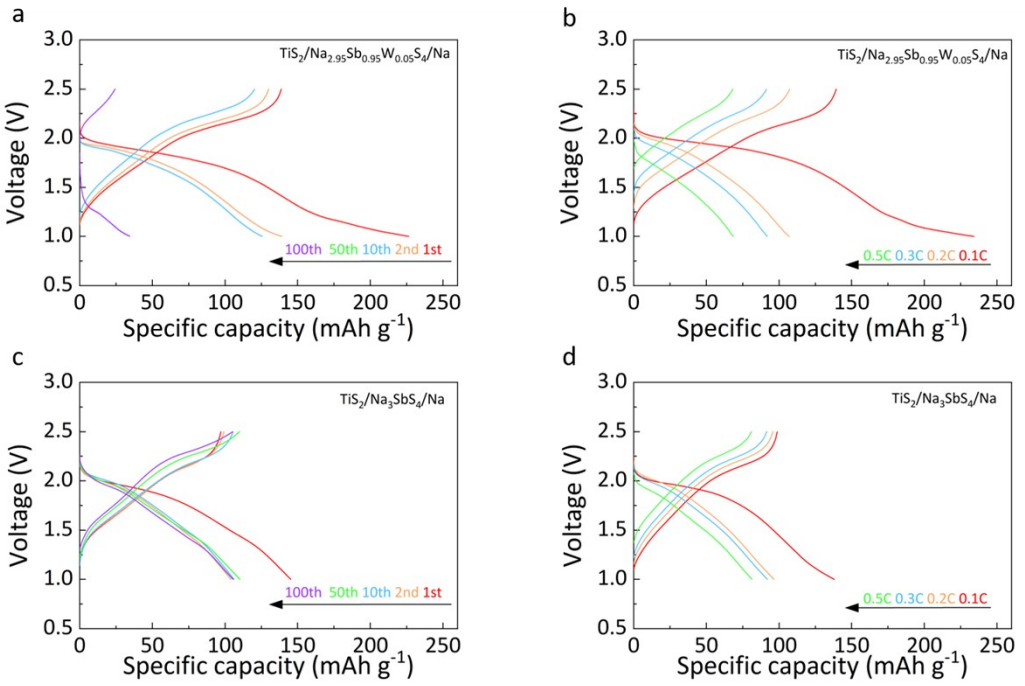

Figure S6. Discharge-charge curves of $TiS_2/Na_{2.95}Sb_{0.95}W_{0.05}S_4/Na$ battery at (a) 0.1 C and (b) different rates from 0.1 to 0.5 C. Discharge-charge curves of $TiS_2/Na_3SbS_4/Na$ battery at (c) 0.1 C and (d) different rates from 0.1 to 0.5 C.

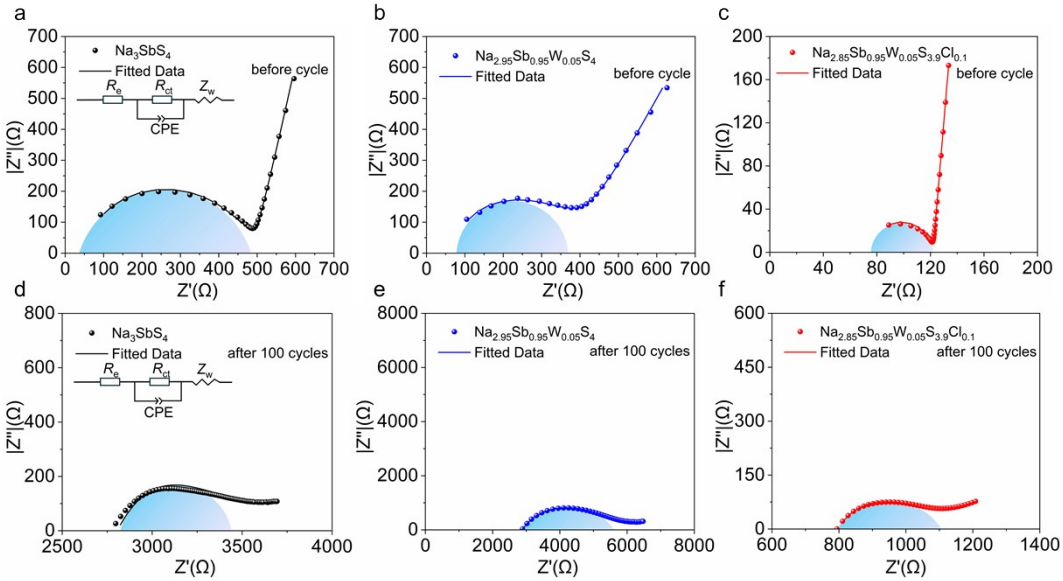

Figure S7 The fitted Nyquist plots of the $TiS_2/Na_3SbS_4/Na$, $TiS_2/Na_{2.95}Sb_{0.95}W_{0.05}S_4/Na$, and $TiS_2/Na_{2.85}Sb_{0.95}W_{0.05}S_{3.9}Cl_{0.1}/Na$ batteries before (a-c) and after (d-f) 100 charge/discharge cycles at 0.1 C.

Table S1. Ionic conductivities of $Na_{3-x}Sb_{1-x}W_xS_4$ solid electrolytes with different dopant contents.

Sample	Dopant content	Z' d^{-1} (Ω mm^{-1})	Area (cm^{-2})	Conductivity (mS cm^{-1})
$Na_{3-x}Sb_{1-x}W_xS_4$	x=0	138.46	0.785	0.92
	x=0.025	16.22	0.785	7.85
	x=0.05	12.71	0.785	10.02
	x=0.075	13.06	0.785	9.75
	x=0.1	18.76	0.785	6.79

Table S2. Ionic conductivities of $Na_{2.95-x}Sb_{0.95}W_{0.05}S_{4-x}Cl_x$ solid electrolytes with different dopant contents.

Sample	Dopant content	Z' d^{-1} (Ω mm^{-1})	Area (cm^{-2})	Conductivity (mS cm^{-1})
$Na_{2.95-x}Sb_{0.95}W_{0.05}S_{4-x}Cl_x$	x=0	12.71	0.785	10.02
	x=0.05	10.22	0.785	12.46
	x=0.1	10.06	0.785	12.66
	x=0.15	12.60	0.785	10.11
	x=0.2	12.93	0.785	9.85

Table S3 Refined structure of Na_3SbS_4.

Lattice parameters	Atom	*x*	*y*	*z*	Occ
	Na1	0.000000	0.500000	0.427115	1.00
$a = b = 7.214$,	Na2	0.000000	0.000000	0.000000	1.00
$c = 7.1861$ (Å)	Sb1	0.000000	0.000000	0.500000	1.00
	S1	0.284185	0.311714	0.151278	1.00

Table S4 Refined structure of $Na_{2.95}Sb_{0.95}W_{0.05}S_4$.

Lattice parameters	Atom	*x*	*y*	*z*	Occ
$a = b = 7.213$, $c = 7.1851$ (Å)	Na1	0.000000	0.500000	0.427115	1.00
	Na2	0.000000	0.000000	0.000000	0.95
	Sb1	0.000000	0.000000	0.500000	0.95
	W1	0.000000	0.000000	0.500000	0.05
	S1	0.284185	0.311714	0.151278	1.00

Table S5 Refined structure of $Na_{2.85}Sb_{0.95}W_{0.05}S_{3.9}Cl_{0.1}$.

Lattice parameters	Atom	*x*	*y*	*z*	Occ
	Na1	0.000000	0.500000	0.427115	1.00
	Na2	0.000000	0.000000	0.000000	0.85
$a = b = 7.213$,	Sb1	0.000000	0.000000	0.500000	0.95
$c = 7.1851$ (Å)	W1	0.000000	0.000000	0.500000	0.50
	S1	0.289617	0.323329	0.158805	0.97
	Cl1	0.289617	0.323329	0.158805	0.03

Table S6 The calculation results of the energy before and after hydrolysis of Na_3SbS_4, W-doped Na_3SbS_4 and W-Cl co-doped Na_3SbS_4 structures

Model	Energy before hydrolysis (eV)	Energy after hydrolysis (eV)
Na_3SbS_4 (a → d)	-527.381	-529.376
W-doped Na_3SbS_4 (b → e)	-533.69	-536.626
W-Cl co-doped Na_3SbS_4 (c → f)	-523.294	-525.15

Table S7. Comparison of ionic conductivity, air stability, and cycling stability of reported W-containing Na_3SbS_4 solid electrolytes.

Solid electrolyte	Ionic Conductivity (mS cm^{-1})	$H_2S(cm^3 \cdot g^{-1})$	Cycling Stability (hour)	reference
$Na_{2.85}Sb_{0.95}W_{0.05}S_{3.9}Cl_{0.1}$	**12.66**	**0.119(120 h,45% RH)**	**>800@0.05mA cm^{-2}**	**This work**
$Na_{2.95}Sb_{0.95}W_{0.05}S_{3.9}O_{0.1}$	8.49		>50@0.1mA cm^{-2}	[S8]
$Na_3Sb_{0.95}W_{0.05}S_{3.95}B_{0.05}$	11.06	0.129(120 h,45% RH)	>500@0.05mA cm^{-2}	[S9]
$Na_{2.804}Sb_{0.879}W_{0.046}S_{3.7}F_{0.075}$	11.13	0.0996(120 h,30% RH)	>800@0.05mA cm^{-2}	[S10]
$Na_3W_{0.15}Sn_{0.15}Sb_{0.7}S_4$	11.30	0.006(30 h,50% RH)	>350@0.1mA cm^{-2}	[S11]

Table S8. The fitted results of EIS plots for $TiS_2/Na_3SbS_4/Na$, $TiS_2/Na_{2.95}Sb_{0.95}W_{0.05}S_4/Na$ and $TiS_2/Na_{2.85}Sb_{0.95}W_{0.05}S_{3.9}Cl_{0.1}/Na$ batteries before and after cycling at 0.1C

Sample	Before cycling		After cycling	
	R_e (Ω)	R_{ct} (Ω)	R_e (Ω)	R_{ct} (Ω)
$TiS_2/Na_3SbS_4/Na$	41.3	441.5	2786.6	615.4
$TiS_2/Na_{2.95}Sb_{0.95}W_{0.05}S_4/Na$	69.1	297.3	2872.2	2704.3
$TiS_2/Na_{2.85}Sb_{0.95}W_{0.05}S_{3.9}Cl_{0.1}/Na$	76.8	44.9	795.4	316.2

References

S1. Hutter, J.; Iannuzzi, M.; Schiffmann, F.; VandeVondele, J., cp2k: atomistic simulations of condensed matter systems. WIREs Computational Molecular Science 2014, 4 (1), 15-25.

S2. Lippert, B. G.; Parrinello, J. H.; Michele, A hybrid Gaussian and plane wave density functional scheme. Molecular Physics 1997, 92 (3), 477-488.

S3. VandeVondele, J.; Krack, M.; Mohamed, F.; Parrinello, M.; Chassaing, T.; Hutter, J., Quickstep: Fast and accurate density functional calculations using a mixed Gaussian and plane waves approach. Computer Physics Communications 2005, 167 (2), 103-128.

S4. Goedecker, S.; Teter, M.; Hutter, J., Separable dual-space Gaussian pseudopotentials. Physical Review B 1996, 54 (3), 1703-1710.

S5. Perdew, J. P.; Burke, K.; Ernzerhof, M., Generalized Gradient Approximation Made Simple. Physical Review Letters 1996, 77 (18), 3865-3868.

S6. Grimme, S.; Antony, J.; Ehrlich, S.; Krieg, H., A consistent and accurate ab initio parametrization of density functional dispersion correction (DFT-D) for the 94 elements H-Pu. The Journal of Chemical Physics 2010, 132 (15), 154104.

S7. Weng, W.; Wan, H.; Liu, G.; Wu, L.; Wu, J.; Yao, X., Liquid-Phase Synthesis of Nanosized Na11Sn2PS12 Solid Electrolytes for Room Temperature All-Solid-State Sodium Batteries. ACS Applied Energy Materials 2021, 4 (2), 1467-1473.

S8. Weng, W.; Liu, G.; Li, Y.; Shen, L.; Yao, X., Tungsten and oxygen co-doped stable tetragonal phase Na_3SbS_4 with ultrahigh ionic conductivity for all-solid-state

sodium batteries. *Applied Materials Today* **2022,** *27*, 101448.

S9. Wang, L.; Liu, G.; Li, Y.; Weng, W.; Xin, X.; Yao, X., Tungsten and Boron Codoping toward High Ionic Conductivity and Stable Sodium Solid Electrolyte for All-Solid-State Sodium Batteries. *Acs Applied Materials & Interfaces* **2024,** *16* (4), 4847-4853.

S10. Wang, L.; Liu, D.; Liu, G.; Pan, H.; Huang, L.; Yao, X., Highly conductive $Na_{2.804}Sb_{0.879}W_{0.046}S_{3.7}F_{0.075}$ with moisture tolerance enables stable all-solid-state sodium batteries. *Nano Energy* **2025,** *142*, 111167.

S11. Huan, T.; Yin, J.; Shen, Y.; Lu, J.; Gao, C.; Liu, Y.; Dai, S.; Lin, C.; Zhang, X.; Ma, H.; Shen, X.; Jiao, Q., Achievement of high ionic conductivity and electrochemical stability by W/Sn-doped Na3SbS4 conductors designed for all-solid-state sodium-ion batteries. Journal of Materials Chemistry C 2024, 12, 19296-19306.